Nat Neurosci. Author manuscript; available in PMC 2014 April 01.

Published in final edited form as:

Nat Neurosci. 2013 October ; 16(10): 1426–1435. doi:10.1038/nn.3499.

Spontaneous cortical activity alternates between motifs defined by regional axonal projections

Majid H. Mohajerani[1,2,6], **Allen W. Chan**[1,2,4,6], **Mostafa Mohsenvand**[1,2], **Jeffrey LeDue**[1,2], **Rui Liu**[1], **David A. McVea**[1,2], **Jamie D. Boyd**[1,2], **Yu Tian Wang**[2,4], **Mark Reimers**[5], and **Timothy H. Murphy**[1,2,3]

[1]Department of Psychiatry, University of British Columbia, Vancouver, BC, Canada

[2]Brain Research Centre, University of British Columbia, Vancouver, BC, Canada

[3]Department of Cellular and Physiological Sciences, University of British Columbia, Vancouver, BC, Canada

[4]Department of Medicine and Vancouver Coastal Health Research Institute, University of British Columbia, Vancouver, BC, Canada

[5]Department of Psychiatry, Virginia Commonwealth University, Richmond, VA, USA

Abstract

In lightly anaesthetized or awake adult mice using millisecond timescale voltage sensitive dye imaging, we show that a palette of sensory-evoked and hemisphere-wide activity motifs are represented in spontaneous activity. These motifs can reflect multiple modes of sensory processing including vision, audition, and touch. Similar cortical networks were found with direct cortical activation using channelrhodopsin-2. Regional analysis of activity spread indicated modality specific sources such as primary sensory areas, and a common posterior-medial cortical sink where sensory activity was extinguished within the parietal association area, and a secondary anterior medial sink within the cingulate/secondary motor cortices for visual stimuli. Correlation analysis between functional circuits and intracortical axonal projections indicated a common framework corresponding to long-range mono-synaptic connections between cortical regions. Maps of intracortical mono-synaptic structural connections predicted hemisphere-wide patterns of spontaneous and sensory-evoked depolarization. We suggest that an intracortical monosynaptic connectome shapes the ebb and flow of spontaneous cortical activity.

Address correspondence to: Timothy H. Murphy. 4N1-2255 Wesbrook Mall, Vancouver, BC, Canada, V6T 1Z3. Fax: (604) 822-7981 (thmurphy@mail.ubc.ca).

[6]Majid H. Mohajerani and Allen W. Chan have contributed equally to this work.

Conflicts of Interest: none

Author Contributions:

M.H.M. and T.H.M. designed the study. M.H.M., A.W.C., D.A.M., and J.L. performed the experiments. M.H.M., A.W.C., M.M, J.L., Y.T.W., and M.R. analyzed the data. M.H.M, R.L., J.L., and J.D.B. participated in processing the Allen Mouse Brain Connectivity data. M.H.M., A.W.C., and T.H.M. wrote the manuscript, which all authors commented and edited. T.H.M. supervised the study.

Introduction

Brain activity related to planned motor output, or sensory information exists on a background of spontaneous activity[1, 2]. This activity shapes behavior during both sensory and motor tasks, but its purpose and composition is unclear[3]. Spontaneous activity within anesthetized cat visual cortex [4] can correspond to functional orientation maps[5]. Although the relationship between spontaneous and evoked activity has been explored within a single sensory modality[5–9], what constrains their behavior within larger cortical circuits is less clear. Recurrent patterns of low frequency (<0.1 Hz) spontaneous activity within larger cortical circuits have been described in rodents, non-human primates, and human subjects using functional magnetic resonance imaging (fMRI)[10–12] and magnetoencephalography[13, 14]. Measurement of both spontaneous and sensory-evoked patterns of fMRI signals were correlated with fiber tracts between brain sulci[10]. Although imaging of fiber tracts has defined major connections, diffusion tensor imaging cannot distinguish unmyelinated fibers or orientation[15] and fMRI has low temporal resolution[1].

We exploit spontaneous cortical activity to provide a continuous sample of active cortical networks assessed using voltage sensitive dye (VSD) imaging. Unlike fMRI and intrinsic optical signal imaging[16, 17], VSD imaging measures electrical activity with relatively high spatial and temporal resolution[18]. VSD imaging has been applied across large regions of the mouse cortex to reveal fast, complex, localized and bilaterally synchronized patterns of depolarization[19]. We examine the extent to which patterns of intracortical spontaneous activity reflect circuits used during sensory processing and their relation to fine cortical structure. To assess the relationship of spontaneous activation patterns to cortical projections, we employ a recent database from the Allen Institute for Brain Science[20]. Analysis of spontaneous activity is advantageous since active arbitrary cortical points can be compared to axonal projections that emanate from the same locations. This strategy works well for areas such as motor cortex, associational areas, or secondary sensory cortex that cannot be directly stimulated by sensation, but are nonetheless an active part of spontaneous activity. We show that spontaneous activity within the naive mouse cortex (1) alternates through patterns of activity that can reflect different sensory modalities (somatosensory, visual, and auditory), and (2) are largely predicted by underlying consensus cortico-cortical monosynaptic axonal projections.

Results

VSD imaging of activity in anesthetized mouse cortex

Using a preparation with a large craniotomy that exposed the right hemisphere (Fig. 1A), we studied interactions between cortical areas using VSD imaging[18]. When stimulating the hindlimb, forelimb, whiskers, visual, or auditory system of lightly anesthetized mice, unique regional patterns of cortical depolarization were observed (Fig. 1B; Supplementary Video 1). All modes of sensory stimulation tested resulted in the initial discrete activation of their primary sensory cortical representation, followed by a non-uniform expansion of depolarization and activation of posterior and midline cortical areas (Fig. 1B and Supplementary Fig. 1). Activity spread involved the recruitment of secondary, non-contiguous areas of cortex. Consistent with previous studies of barrel cortex, we found that

brief tactile stimulation of C2 whisker activated primary somatosensory areas as well as "islands" of response within functionally related areas such as primary motor cortex (M1)[6, 21–23], and secondary representation of somatosensory cortex (S2) (Fig. 1Bi)[22]. Auditory stimulation resulted in activation of primary auditory cortex (A1) and secondary activation of cortex centered on the parietal association area (ptA) (Fig. 1Bii). Stimulation of forelimb and hindlimb resulted in activation of their respective primary somatosensory areas (FLS1&HLS1) and recruitment of secondary somatosensory cortices (FLS2&HLS2) (Fig. 1Biii–iv). Visual stimulation activated primary (V1) followed by spread of activity to secondary visual cortices (V2) and also recruited midline cortical areas including anterior cingulate/secondary motor cortex (AC/M2), and retrosplenial cortex (RS) (Fig. 1Bv). Activation of primary visual cortex and associated midline areas within the opposite hemisphere (ipsilateral hemisphere) was observed after a delay (Fig. 1C). Notably, we observed patterns of spontaneous activity that resemble those during sensory stimulation (Fig. 1D; Supplementary Video 2).

Consistent with recent findings[24], RH-1692 (voltage sensitive dye) incubation increased the LFP response to sensory stimulation (Fig. 1E,F); importantly this effect does not appear to be due to general disinhibition since spontaneous activity assessed by LFP or EEG was not affected (Fig. 1G,H and Supplementary Fig. 2C,D). In addition, we note that the magnitude of RH-1692 facilitation of sensory-evoked responses falls within the range of excitability changes observed from the effect of anesthesia on the amplitude of sensory-evoked responses (Supplementary Fig. 2F). We mention RH-1692 facilitation as a potential caveat of these studies, but argue that in the absence of an experimental model of widespread cortical expression of voltage sensitive fluorescent protein[25], that this may be the best available means of imaging of widespread cortical activity.

We quantified the sensory-evoked spread of VSD activation using a Combined Local-Global Method of optical flow measurement[26]. A similar approach was used previously to quantify VSD cortical dynamics[27]. Direction and velocity of cortical depolarization were determined for each image following stimulation (Fig. 2Ai and Supplementary Video 3). Maximum velocity measurements (Fig. 2Aii and Supplementary Video 3) were derived for patterns of activity induced for each mode of stimulation. The movement of maximum velocity position during activity spread was plotted over the cortex (Fig. 2B) and indicated stimulus specific source locations, at the associated primary sensory cortices, followed by movement of the responses toward more medial areas (Fig. 2B). While source locations were stimulus specific, there was a common sink location within the parietal association area (ptA) for activity induced by sensory stimulation (Fig. 2C). Visual stimulation exhibited a second more anterior sink location near AC/M2 (Fig. 2C).

To assess whether the spread of activation was derived from consensus intracortical circuits (that were independent of sensory processing) we repeated optical flow analysis for intracortical activity stimulated by channelrhodopsin-2 (ChR2) within Thy-1 transgenic mice[22]. The characteristics of activity spread were similar with respect to whether it was induced by sensory stimulation (whisker or forelimb), or by direct ChR2-mediated activation of the associated primary sensory cortices (BCS1 or FLS1) (Fig. 2D). Consistent with this

observation, sink locations for activity spread from sensory stimulation or photostimulation of the cortex were also similar (Fig. 2E).

Diverse activity sources create similar correlation maps

In anesthetized mouse, spontaneous cortical activity is dominated by slow-wave activity with greatly reduced power at higher frequency bands[19](Supplementary Fig. 2). By examining sequences of slow-wave spontaneous cortical activity (0.1–6 Hz) using VSD imaging in anesthetized mice, we noticed regional patterns that at times resembled those present from averaged trials of sensory stimulation (Fig. 1D and Supplementary Video 2). Spontaneous slow wave activity was recorded in the absence of external stimulation to sensory systems using equipment that did not produce discernible vibration or auditory stimulation[19]. Red light used to excite VSD fluorescence was directed away from the eyes and continuously applied to avoid intermittent stimulation[19]. To analyze patterns of spontaneous activity quantitatively we made correlation maps based on a seed-pixel within the center of a distinct cortical area (see Methods) similar to seed-voxel correlation analysis used in resting-state fMRI data to detect functional connectivity[28]. Using a seed-pixel within the primary representation of forelimb somatosensory cortex (FLS1) in anesthetized mouse, we examined its correlation to all other pixels within the imaged cortex during a 300 s period (6.7 ms frames, 0.1–6 Hz) of spontaneous activity (sFLS1, Fig. 3A). Supplementary Video 4 shows cumulative seed-pixel based correlation maps for the forelimb cortex alongside the spontaneous activity used to create them. The correlation values in the map are highest around the seed-pixel and included areas that are functionally related over the period chosen to measure spontaneous activity. Comparison of these spontaneous or sensory-evoked correlation maps using spatial correlation analysis indicated similarity (Supplementary Figs. 3 and 4). With respect to hindlimb cortex, correlation maps generated from time-series of spontaneous activity with seed-pixels within hindlimb cortex (sHLS1) were similar to the correlation map generated from hindlimb sensory-evoked activity (eHLS1) (Fig. 3B) (Supplementary Figs. 3 and 4). Similar approaches were used for comparison of correlation maps obtained from spontaneous and evoked activity within other sensory modalities such as audition (Supplementary Fig. 4E and 5A), vision (Supplementary Fig. 4F) and vibrissa-sensation (Fig. 3C, Supplementary Fig. 3 and 4B), or regions that were not selectively accessible by peripheral sensory stimulation such as secondary representation of sensory cortices (Fig. 3D and Supplementary Fig. 5A). To control for the contribution of correlation coefficient values near the seed-pixel location, we subtracted these values prior to spatial correlation analysis (See Methods). In this manner, we excluded local functional connections and focused exclusively on second order, distant connections. In all cases, there was strong correspondence between the correlation maps of spontaneous and sensory-evoked activity belonging to the same cortical location (Supplementary Fig. 3B).

We repeated the seed-pixel correlation analysis for intracortical evoked activity stimulated by ChR2 [22] to assess whether these correlations were derived from consensus intracortical circuits that were independent of sensory processing. Optogenetic stimulation of a cortical area closely resembled spontaneous activity patterns that involved that area, or sensory stimulation (Fig. 3). Seed-pixel correlation maps generated from VSD imaging of spontaneous, sensory-evoked, or photostimulation-evoked cortical activity indicated

similarity between the 3 types of maps (Supplementary Fig. 3B). This is consistent with similarity we have observed using region of interest-based correlation analysis (Supplementary Fig. 4). In contrast, when maps were compared across different sensory cortices significant differences were observed (Supplementary Fig. 3B). Correlation maps were not obtained after application of 30 μM tetrodotoxin (TTX) to the cortex indicating dependence on neuronal activity and that correlation due to other factors is low (Supplementary Figs. 5C,D). As expected, shuffling of pixel values within each frame of imaged cortex, prior to seed-pixel correlation analysis, failed to produce these maps (Supplementary Fig. 5E,F). Distinct correlation maps of both spontaneous and sensory-evoked activity were apparent even when neighboring cortical regions at a distance of only 0.5 mm were examined providing a minimum estimate of VSD spatial resolution (Supplementary Fig. 5A,B).

VSD imaging of cortical activity in quiet awake mice

The results in Fig. 1–3 and Supplementary Figs. 1–6 were obtained from mice under isoflurane anesthesia to reduce movement artifacts or activity related to voluntary behavior. In awake rodents engaged in specific tasks such as whisking, cortical spontaneous activity is desynchronized[3, 29] and the cortical responses exhibit enhanced synaptic inhibition[30]. In contrast, cortical neurons of quiet awake rodents exhibit oscillations that are synchronized both locally[8, 29] and across hemispheres[19]. We examined whether sensory stimulation or spontaneous activity in quiet awake mice evoked similar, stereotypical patterns of activity as those observed in anesthetized mice. We imaged both spontaneous and sensory-evoked cortical activity in head-fixed, awake mice and also in subsequently isoflurane-anesthetized mice. Using a second camera to monitor animal movements (mainly forepaw and whiskers) and muscle tone measurement through an EMG electrode inserted in the neck, we classified the animal's state into anesthetized, or quiet wakefulness (Fig. 4A and Supplementary Fig. 2E). Under these conditions we show the spatiotemporal dynamics of activity in response to sensory stimulation (visual or auditory) and during spontaneous activity under conditions of isoflurane anesthesia or in quiet awake states (Fig. 4B, E). Quantification of sensory-evoked VSD response parameters, such as peak amplitude and time to peak, in anesthetized and quiet awake states measured from center of V1 or A1 did not show significant differences (Fig. 4B–D). In both anesthetized and quiet awake states we observed activation of distant areas such as ptA and M2/CG areas for auditory and visual stimulation respectively (Fig. 4B–D and Supplementary Video 5).

Region-specific intracortical seed-pixel correlation maps generated from spontaneous or sensory evoked activity were similar in anesthetized and quiet awake mice (Fig. 5 and Supplementary Fig. 3C). These data suggest that functional connectivity can be inferred from data using light isoflurane anesthesia.

Reverberation of sensory motifs in spontaneous activity

To characterize the distribution of spontaneous activity motif repeats over time we employed a whole frame spatial correlation approach where sequences of spontaneous activity were compared to templates that reflect the onset of cortical activation[5], created from average VSD activity patterns evoked by multiple modes of sensation (Fig. 6A, see Methods). This

analysis yielded a single correlation value for the comparison of each image frame of spontaneous activity with an image template (Fig. 6B). Hindlimb, forelimb, auditory, whisker, or visual stimulation templates were correlated to 30 s of spontaneous activity in isoflurane anesthetized animals yielding plots of correlation coefficient versus time (Fig. 6B–C). Within these time plots peaks were observed where selected sequences of spontaneous activity closely resembled sensory template images (Fig. 6Bi–v). These cortical activity motifs within spontaneous activity were found to repeat when prolonged sequences of spontaneous activity were examined (Fig. 6C). At times spontaneous activity exclusively resembled a single sensory modality response, while at other times overlap was apparent between multiple sensory modalities. Repeats of cortical activity motifs were apparent at much lower rates when motifs derived from randomly placed blobs that resembled cortical activity were used as templates (Supplementary Fig. 6B–D). Also, as expected sensory motifs were not present in spatially shuffled data (Supplementary Fig. 6E–F).

To estimate the fraction of variance associated with cortical sensory motifs we used a regression approach employing 5 separate sensory motifs and found that these motifs accounted for 18.5±1.1% (mean ± s.e.m.) of total VSD signal variance of spontaneous activity (0.1–6 Hz bandpass filtered; n=7 mice). Given that there are likely more than 5 sensory motifs, and likely many for non-sensory activity, this represents a lower limit. As a further test of repeating motifs within spontaneous activity, we used a sensory template composed of the first 3 frames following the initial VSD response and found general agreement with the results obtained from a single image, but that the peak correlations were blunted (Fig. 6D and Supplementary Video 6 and 7). Three frame templates were able to recover modality-specific patterns from spontaneous activity that resembled sensory responses but at a slower timescale (Supplementary Fig. 1C, Supplementary Video 6 and 7).

Cortical axonal projections and functional connectivity

To assess how the regional patterns of VSD response were related to underlying structural circuits, we examined the Allen Mouse Brain Connectivity (AMBC) Atlas. The atlas provides axonal projections that are labeled with the anterograde tracer GFP expressed using adeno-associated virus (AAV) injection into discrete cortical locations and brain nuclei of C57BL/6 mice[20]. These mice were the same strain and age range of the animals used in our study. We have chosen to make comparisons between spontaneous activity patterns and axonal projections since the seed-pixel correlation method allowed us to determine regional functional connectivity associated with the same sites that were targeted by the AMBC for injection of AAVs. Although both axons and dendrites were labeled with GFP, we quantified projections >0.5 mm from the AAV injection site center, that were mostly long-range axonal projections. We have taken this 3D structural data and processed it to match the perspective of our 2D VSD images as shown in Fig. 7A.

By examining axonal projections in 2D flattened representations of the AMBC Atlas which emanated from primary trunk cortex and comparing these to the correlation map of spontaneous VSD activity for the same region measured from anesthetized mice, we observed strong spatial co-localization (Fig. 7B). Furthermore, similar co-localization was observed within the primary motor cortex (Fig. 7B) and other examined regions (Fig. 8A

and Supplementary Fig. 7C–F). Maps of axonal projections and VSD correlation maps were co-localized (based on spontaneous cortical activity) for injections that target the same cortical area within different animals (Supplementary Fig. 7A,B). Since some local correlation between structure and function would be apparent due to local spread of AAV labeling around the injection site, we removed the area centered over the injection or seed-pixel used in correlation analysis of functional data using a Gaussian fit and subtraction procedure when making statistical comparisons (Supplementary Fig. 8). Local correlation attributed to non-biological sources such as image sampling were examined and the point spread function was estimated to be <67 μm (1 pixel). Spatial correlation of axonal projections for 9 cortical areas were compared with the corresponding functional correlation maps determined by VSD imaging (Fig. 8B; n=7). It should be noted that although the VSD correlation maps for ptA were most similar to the structural map of ptA axonal projection, the RS map for structural connectivity also showed a high value of correlation since axons within these two regions overlap (Fig. 8A–B and Supplementary Fig. 7C,F). As an alternative means of comparing structural and functional of cortical connectivity, we used a region of interest based analysis. When we compared the strength of parietal association cortex axonal projections to eleven ROIs of functional correlation maps measured using VSD imaging of spontaneous activity, or seed-pixel correlation analysis of photostimulation-evoked responses (Fig. 8C and Supplementary Fig. 9 for additional cortical regions), we provide evidence that a significant amount of VSD cortical dynamics were explained by underlying patterns of monosynaptic axonal projections.

When axonal projection maps of labeled neurons within different injection locations were differentiated into the supragranular layers I–III versus infragranular layers V–VI, we found that the axonal projection maps were similar across cortical laminae (Supplementary Fig. 10). It is therefore plausible to use VSD imaging that mainly detects superficial cortical activity[18] for comparison to maps extracted from axonal tracing results from all layers.

Discussion

VSD imaging of cortical activation motifs

We employ VSD imaging to monitor cortical activity over rapid physiologically relevant timescales[18,5, 6, 9, 19, 22, 31, 32]. The approach permits the comparison of these functional networks to underlying axonal mono-synaptic projection structure[20]. We demonstrate unique regional cortical motifs associated with forms of sensory stimulation and the ability of spontaneous activity to contain representations of these widespread circuits. We observe that sensory, photostimulation-induced, or spontaneous activation leads to intracortical spread of the VSD depolarizing response. This result may seem to be at variance with the idea that sensory activation should be relatively restricted and primarily limited to somatotopic areas[33]. However, VSD imaging can detect both sub-threshold and supra-threshold activity[18]. Given the relatively long time course of sub-threshold events, their contribution to VSD signals can be significant and may indicate a modulatory role[16, 33].

The observation of extensive intracortical spread of depolarization is consistent with previous intrinsic signal optical imaging combined with electrophysiological recording data from the somatosensory and auditory cortices[16]. Likewise, voltage sensitive fluorescent

protein imaging reveals spread of depolarization resulting from sensory stimulation to extend several millimeters[25]. Although depolarizing events can spread over a considerable distance, they nonetheless exhibit specificity. In examining different forms of sensory stimulation we observe modality-specific cortical activation patterns. For example visual stimuli lead to V1 activation, and auditory stimuli lead to A1 activation with relatively short latency. At later times divergent sensory stimuli lead to common patterns of activation that include ptA and midline activation (M2/AC and RS areas). The propagation of sensory-evoked activity along these midline routes and frequent activation of these same regions by spontaneous activity[19] suggests that these regions are hubs within the mouse cortex[22], in which multiple forms of sensory information integrate during both evoked and spontaneous cortical activity. The spread of activation to sinks within posterior midline areas such as ptA is consistent with similar areas forming a connectional core within human brain[1].

State dependence of cortical activity motifs

We report patterns of intracortical spontaneous and sensory-evoked activity for quiet awake and lightly anesthetized animals. The spread of activity from primary activation areas to distant but anatomically and functionally connected regions (for example anterior cingulate for visual stimuli and parietal association cortex for auditory stimulation), became stronger in the awake state. This awake state-dependent increase of functional connectivity may be essential for integration of multisensory information and perception[3]. It is likely that subtleties within cortical state associated with different behaviors will modify the regional patterns we observe[3, 29]. Ultimately, functional studies will need to be conducted under specific scenarios to examine additional state-dependent connectivity relationships[3, 8, 19, 34]. However, similarity in connectivity patterns between quiet awake and anesthetized data, and their relationship to the core structural connections suggests that major activity patterns under anesthesia will likely translate to different cortical states associated with active task engagement[3, 10].

Although similar correlation maps were observed between quiet awake and anesthetized states, recent data indicates that during wakefulness, cortical responses exhibit enhanced synaptic inhibition that may restrict the spatiotemporal structure of evoked responses[30]. Similarities in correlation maps for quiet awake and anesthetized activity likely reflect strong consensus intracortical pathways and do not necessarily imply that these two brain states employ identical temporal or microscopic circuit features.

Spontaneous activity is a resource of circuit activity

We have exploited spontaneous activity to provide a rich palette of cortical activity that can be captured by VSD imaging. Advantages of using this approach include the ability of cortical circuits to be sampled in a repeated manner, and even with multiple response patterns occurring concurrently. Furthermore, the analysis of spontaneous activity allows the simultaneous observation of functional connectivity of sensory regions as well as arbitrary points that cannot be directly activated by sensory stimulation. The advantage of using spontaneous activity and single pixel-based correlation analysis is that we can derive functional relationships for any site that was targeted by AAV injection.

To establish associations between the AMBC atlas injection sites and the equivalent functional sites, we have employed functional landmarks for alignment such as the center of V1 or A1 that are experimentally defined by sensory stimulation and are present within the AMBC atlas structural data set, as well as anatomical landmarks. There could be errors in positioning, although the use of functional and anatomical landmarks should minimize them. Given the close correspondence between spontaneous and evoked activity response patterns, we do not anticipate major differences in functional connectivity maps if evoked activity were used instead of spontaneous activity for comparison with anatomical connectivity maps.

Spontaneous activity contains motifs of sensory activity

We demonstrate that repeating circuit motifs used during sensory processing are present in spontaneous activity. This concept may be similar to a recall of patterned activity within memory tasks observed in the hippocampus and prefrontal cortex[35, 36]. To identify cortical motifs we have used a single image that reflects the onset time of sensory responses. Although templates based on multiple images may be more stringent, the eventual flow of activity from initial selective points to more general cortical sinks degrades specificity. Further analysis of images using independent component analysis[1, 28] may be informative for decomposing spontaneous activity into multiple network maps that group correlated regions together.

Although we have described the contribution of sensory motifs to cortical spontaneous activity, it is likely that unique motifs associated with non-sensory activity are also present. Currently we have a limited understanding of activity motifs associated with higher cognitive function[1]. We anticipate that these motifs may be defined using specific behavioral assays[1, 6], or perhaps optogenetics to directly activate subsets of these circuits[22].

Relation of activity propagation to axonal projections

Surprisingly records of VSD co-activation are highly correlated with monosynaptic axonal projections. The distances over which we observe intracortical VSD signal propagation are on the order of 0.5–6 mm, within the range of monosynaptic intracortical axonal projections[37]. This suggests that the major horizontal architecture of cortex for relaying information over rapid timescales may predominantly involve single projections. This is consistent with previous work done in barrel cortex [6, 23] and extended by us to additional regions of brain and, in particular associational areas that cannot be studied using sensory stimulation. Although long range relays are single projections, once this activity arrives at its destination it is likely distributed to a columnar canonical cortical microcircuit[37, 38]. The correlation analysis we have performed assumed little or no lag between different regions of cortex. We highlight short latency relationships, although it is possible that by adding negative or positive time lags to the correlation analysis[39] that both upstream or downstream circuits may be studied.

We show similarity between functional connectivity maps obtained from patterns of VSD signal and maps of structural connectivity, although we caution that there is not a linear relationship between projection intensity and the strength of functional connections

determined by VSD activity. For comparison of these quantities we have used a spatial correlation analysis for VSD signals versus linear or log transformed values of axonal projection intensity. In this case given the dissimilar quantities being compared we suggest caution regarding quantitative statements about the relationship between VSD correlation coefficient maps and axonal projection intensity. Instead, we examine the relative spatial distribution of each. Projection maps illustrating long range axonal connections can sometimes appear discontinuous with gaps between the source and target areas. The target areas within these maps represent terminal axonal arbors that are connected over long distances through axonal projections which transit the sub-cortical white matter consistent with anatomical studies. The emergence of ascending axons and their arbors toward superficial layers may contribute to the apparent similarity in supragranular and infragranular anatomical maps. However, this does not imply that there are not important differences between deep and superficial cortical circuitry, but rather they were not observed at our level of assessment. An alternative model for traveling wave propagation is through bidirectional cortical-thalamic loops[33, 40]. Although most VSD response patterns we observe are consistent with underlying cortical structural projections, we cannot exclude a role for cortical-subcortical loops[41].

Our current work compares VSD response patterns to structural projections made using monosynaptic anterograde tracers. With the use of retrograde polysynaptic rabies virus tracers[42], it would be possible to target multi-synaptic pathways. These experiments could also involve rabies viruses that permit both structural and functional analysis using optogenetic tools to manipulate upstream projections[43].

Although we argue that much of cortical functional architecture can be described through these apparently excitatory projections, we do not exclude a role for intracortical inhibitory circuits[44] in shaping these signals. However, most inhibitory projections do not span long distances[45]. More detailed analysis of cortical activity[46] will likely reveal cortical layer specific functional connections that may be influenced by local intracortical inhibition. We used positive correlation to examine areas that are co-activated. It may also be possible to examine areas that are negatively correlated where one region may inhibit another[45].

We have been fortunate that the AMBC dataset is derived from C57BL/6 mouse that we employ. Studies of cortical connection structure[47–49] and function could be extended to animals that model disease. Investigators have begun to develop hardware to stimulate circuits that were lost due to ischemic damage[50]. Brain stimulation may be aided by knowledge of cortical functional connections leading to rationally designed stimulus paradigms that could be translated to patients using transcranial magnetic stimulations, transcranial direct current, or even optogenetics.

Methods

Animals

Adult (~25 g) male C57BL6J mice were used (n= 30), for most experiments, while adult male (~25 g) (n=7) ChR2 transgenic mice (line 18, stock 007612, strain B6.Cg-Tg (Thy1-COP4/EYFP) 18Gfng/J; the Jackson Laboratory) were used for a subset of these

experiments. Animals were housed in clear plastic cages in groups of two to five, under a 12:12 h light/dark cycle. Mice were given *ad libitum* access to water and standard laboratory mouse diet at all times. Animals used in awake imaging experiments were housed singly following head-restraint implantation surgery. Animal protocols were approved by the University of British Columbia Animal Care Committee and were in accordance with guidelines set forth by the Canadian Council for Animal Care.

Surgery

At approximately 16 weeks of age, mice were given a craniotomy. Mice were anesthetized with isoflurane (1.0–1.5%), for induction and during surgery, while a reduced maintenance concentration of isoflurane (0.5%) was used later during data collection. Mice were placed on a metal plate that could be mounted onto the stage of the upright macroscope and the skull was fastened to a steel plate. A 7×6 mm unilateral craniotomy (bregma 2.5 to −4.5 mm, lateral 0 to 6 mm) was made and the underlying dura was removed, as described previously[19]. Throughout surgery and imaging, body temperature was maintained at 37°C degrees using a heating pad with a feedback thermistor. In some cases, mice were also given a tracheotomy to assist with breathing.

VSD Imaging

For *in vivo* VSD imaging, the dye RH1692 (Optical Imaging, New York, NY)[51], was dissolved in HEPES-buffered saline solution (1 mg/ml) and applied to the exposed cortex for 60–90 min, staining all neocortical layers, as reported previously [19]. VSD imaging began ~30 minutes following washing unbounded VSD. To minimize movement artifacts due to respiration, the brain was covered with 1.5% agarose made in HEPES-buffered saline and sealed with a glass coverslip. For VSD data collection, 12-bit images were captured with either 5 or 6.67 ms temporal resolution with a CCD camera (1M60 Pantera, Dalsa, Waterloo, ON) and EPIX E4DB frame grabber with XCAP 3.1 imaging software (EPIX, Inc., Buffalo Grove IL). VSD was excited with a red LED (Luxeon K2, 627 nm center), and excitation filters 630 ± 15 nm as described [19]. Images were taken through a macroscope composed of front-to-front video lenses (8.6 × 8.6 mm field of view, 67 μm per pixel). The depth of field of our imaging setup was 1 mm [22]. VSD fluorescence was filtered using a 673–703 nm bandpass optical filter (Semrock, New York, NY). Since animal brain state exhibit spontaneous change [19], we averaged 10–45 trials of stimulus presentation to reduce these effects. To correct for time-dependent changes in VSD signals that accompany all imaging, we also collected a number of non-stimulation trials that were used for normalization of stimulated data. A 10 s interval between each sensory stimulation was used. To reduce potential VSD signal distortion caused by the presence of large cortical blood vessels, we focused into the cortex to a depth of ~1 mm. In our previous work, we measured VSD fluorescence across the cortex using histology and demonstrated relatively high labeling at even ~750 μm in depth [19]. Nonetheless, to reduce regional bias in VSD signal caused by uneven dye loading or due to brain curvature, all VSD responses were expressed as a percent change relative to baseline VSD responses ($\Delta F/F_0$*100%) using Matlab (Mathworks, Natick, MA). VSD imaging of spontaneous activity was performed in the absence of visual, olfactory, tactile, or auditory stimulation during 30s epochs with 6.67 ms (150 Hz) temporal resolution. Slow, time-dependent reductions in VSD fluorescence were corrected in Matlab

using a zero-phase lag Chebyshev bandpass filter (zero-phase filter) at 0.1 – 6 Hz. Ambient light resulting from VSD excitation (630 nm) was measured at 8.65×10^{-3} W/m^2. Total duration of VSD excitation in a typical imaging experiment ranged from 900–1200 s. VSD $\Delta F/F_0$ (%) and cortical EEG power were stable during recordings of up to 25 min (Supplementary Fig. 2C,D) indicated little phototoxicity under the conditions we employ. The fluorescence changes were quantified as $(F-F_0)/F_0*100$ where F represents the fluorescence signal at any given time and F_0 represents the average of fluorescence over all frames.

VSD imaging in awake animals

Young (8–10 weeks old) male C57BL/6 mice (n = 6) were surgically implanted with a plastic screw [19] on the skull for immobilization by connecting to a fixed connector. After 7d of recovery, mice were habituated to head restraint, as described previously[19], and situated on top of running wheel. Once habituated, a 7 × 6 mm craniotomy was performed under isoflurane anesthesia (0.5–2% maintenance mixed with oxygen) and then transferred to an awake imaging setup in which they were head restrained in a relaxed posture. To wake the animals, the isoflurane and oxygen were stopped, the anesthesia mask was removed, and VSD imaging data was obtained over the next 1–2 h. Animal body temperature was maintained with heat lamp. Awake VSD imaging of spontaneous activity imaging was performed in the absence of visual and auditory stimulation during 30 s epochs. The 627 nm LED light used for VSD excitation or the infrared light used for behavioral observation did not result in a visual response. The use of behavioral monitoring camera confirmed that the animals were indeed awake and relatively unstressed since grooming, whisking, walking, and running were observed. Following image acquisition in the awake state, animals were anesthetized with isoflurane, and spontaneous and sensory-evoked activity were recorded in the lightly anesthetized state. An analgesic, buprenorphine, was injected (0.075 mg/kg, i.p.) 24 h before awake VSD recording. We used a second Dalsa 1M60 camera (150 Hz) to capture body and whisker movements under infrared illumination.

Cortical EEG recording

A Teflon coated, chlorided silver wire (0.125 mm) was placed on the right edge of the craniotomy. A reference electrode was placed on the nasal bone. The cortical signal was amplified (1000x) and filtered (0.1–1000 Hz), using an AM Systems (Sequim, WA) Model 1700 AC amplifier.

LFP recording

A silicon multielectrode (NeuroNexus Technologies) was used for recording LFP. The LFP signal was amplified (1000x) and filtered (0.1–1000 Hz) using 16-channel data acquisition system (USB-ME16-FAI-System, Multi Channel Systems).

EMG recording

A Teflon coated, chlorided silver wire (0.125 mm) was fixed using conductive glue to a thin acupuncture needle (0.14 mm) and inserted into neck muscles. A reference electrode was

placed on the back of the animal under the skin. The EMG signal was amplified (1000x) and filtered (1–1000 Hz), using an A-M Systems (Sequim, WA) Model 1700 AC amplifier.

Sensory stimulation

Sensory stimuli were used to generate maps of sensory cortical areas, in no particular order, forelimb (FL), hindlimb (HL), whisker (WK), visual (VL), and auditory (AD) stimulation. To stimulate FL and HL, thin acupuncture needles (0.14 mm) were inserted into the paws and a 0.2–1 mA, 1 ms electrical pulse was delivered. To stimulate a single whisker (C2), whisker was attached to a piezoelectric device (Q220-A4-203YB, Piezo Systems, Inc., Woburn, MA), and given a single 1 ms tap using a square pulse. The whisker was moved at most 90 μm in an anterior to posterior direction, which corresponds to a 2.6° angle of deflection. A 1 ms pulse of combined green and blue light was delivered as visual stimulation. A single 1 ms tone (25 kHz) was used as auditory stimulation. Averages of sensory stimulation were calculated from 10–40 trials of stimulation with an interstimulus interval of 10 s.

Photostimulation

A diode pumped solid state laser emitting 473 nm light (CNI Optoelectronics, Changchun, China), was used to stimulate ChR2-expressing neurons. The beam was positioned on the cortex using custom software written in IGOR PRO (Portland, OR), which controlled galvanometer scan mirrors (Cambridge Tech, Lexington, MA), via analog output voltage from PCI-6110 DAQ (National Instruments, Austin, TX), as reported previously[22]. The beam diameter measured through the objective was 70 ^m and was nearly collimated. The IGOR program controlled the overall timing of individual stimulation trials with TTL triggers to XCAP software. Low amplitude and short duration single laser pulses were used to ensure sufficient activation and a low laser stimulus artifact (2.5–5 mW, 1 ms pulse). Consistent with previous data, this brief activation led to EEG depolarization[22]. Nineteen regions of interest (ROIs) were selected for photostimulation. All regions were targeted for semi-random photostimulation for a total of 19 stimulation sites in one hemisphere. Each site was stimulated 5–10 times (10s interstimulus interval) and replicate responses were averaged together[22].

Data Analysis

For region-based correlation analysis (Supplementary Fig. 4), 18, 5x5 pixel ROIs were selected. Sensory stimulation was used to determine the coordinates for the primary sensory areas (HLS1, FLS1, BCS1, V1, and A1), secondary somatosensory areas (HLS2, FLS2, and BCS2), and primary motor cortex for whisker. From these primary sensory coordinates, the relative locations of additional associational areas were estimated using stereotaxic coordinates[52] (ptA, RS, M2, V2M, V2L, mHL, and mFL).

To calculate the similarity between the spontaneous and cortical response to different forms of sensory stimulation, we first created templates of different forms of sensory activity by taking the initial segment of VSD evoked responses (Fig. 6A). Then, we calculated the correlation coefficient (correlation index) between the templates and each individual frame of spontaneous activity. Frames of spontaneous activity with a correlation coefficient greater

than a given threshold were considered to be a “match” to the evoked templates. To determine the threshold value, we calculated the maximum of correlation coefficients between all sensory templates (hindlimb, forelimb, visual, auditory, and whisker) and the results were multiplied to a constant factor (1.34). To find the constant factor, we measured the percentage of matched hindlimb template, as a function of different constant factor for 7 experiments (Supplementary Fig. 6A). The resulting plot (black) was fitted with an exponential curve (red). We chose the curve decay constant (blue dash line) as a constant factor (e^{-1}). For multiple-frame template search, the first three frames following initial activation of sensory cortex were used (Fig. 6A, D). To create seed-pixel correlation maps (Figs. 3, 5, 7, 8 and Supplementary Figs. 3, 5 and 7), we calculated the zero-lag Pearson product-moment correlation between the VSD signal time course extracted from a ‘seed’ pixel of interest and every pixel within the imaging area. The length of activity used to calculate the correlation index were 300 s for spontaneous activity and 510 ms for sensory-evoked and photostimulation-evoked responses.

Optical Flow Analysis

Optical flow approaches calculate vector fields which determine the apparent velocities of objects in time varying image sequences[26]. We used a Combined Local-Global algorithm developed using a Matlab toolbox to quantify the trajectory of maximum velocity position at various time points following sensory and photostimulation-evoked VSD activity. The detailed description of the Combined Local-Global algorithm is documented previously[26]. The Matlab toolbox is available to download (http://people.csail.mit.edu/celiu/OpticalFlow/). We used Mathematica software (Wolfram Research, IL) built-in “ListStreamPlot” function to calculate streamlines which uses a high order Runge-Kutta method. We used this analysis to identify sink and source locations on the cortex. We calculated the outgoing or ingoing flow in small closed regions which can be performed by numerical realization of divergence operator ($\nabla \cdot \boldsymbol{V}$), where $\boldsymbol{V}$ is the velocity vector. Using this approach, regions with highly positive or negative total flow can be recognized as sources or sinks of the vector field. Pre-smoothing iterations to find the singularities of the velocity vector fields were performed prior to numerical flow calculation.

Pharmacology

For pharmacological experiments, the cortex was covered with HEPES-buffered saline solution to allow for later topical application of 30 μM tetrodotoxin (TTX). The cortex was incubated with TTX for 30 min prior to further imaging.

Statistics

For the composite data shown in Figs. 4, 8 and Supplementary Figs. 2, 3, 5, and 6. we used a one-way ANOVA and a Bonferroni post-hoc analysis. For the composite data in Figs. 2 and Supplementary Figs. 1 and 4, we used the following test. First, we determined locations of maximal activation for each mouse independently. Then we computed the (vector) mean and variance of maximal activation across mice. Then we subtracted each of the two coordinates from the mean for each pair of sensory modalities and divided by the squared standard error of the means.

$$F_{i,j,k,t}=\frac{\left(\overline{x}_k^i-\overline{x}_k^j\right)^2}{\frac{\left(s_k^i\right)^2}{n}+\frac{\left(s_k^j\right)^2}{n}}$$

Where *i, j* index the sensory modality, *k*=1,2 index the coordinate (horizontal or vertical), *t* index the time step, and *n* is the number of mice used (usually 7). Under the null hypothesis these ratios would have an *F(1,n−1)* distribution. We then compute the sum of these *F*-scores over coordinates *k* and time steps *t* (5 steps).

$$F_{i,j,k}^*=\sum_{t=1}^{5}F_{i,j,k,t}$$

There is no analytic expression for distribution of a sum of independent F-scores. We therefore simulated the distribution of such scores by generating independent draws from *F*(1,6) distributions and adding them in groups of five of them to obtain a distribution of *F** under the null hypothesis of no difference in trajectories. We did 10,000 draws and set our threshold at $p< 0.001$, the largest score from this simulation. We followed the same strategy for showing that there was no significant difference in the sink of each sensory modality, except that there was no dependence on t.

There are several places in which correlations are used in this paper to make comparison within and across animals. In Figs. 3, 5 and Supplementary Fig. 5 (group analysis in Supplementary Figs. 3, and 5), we computed seed pixel correlation maps using temporal correlation of data obtained from different origin of activity (spontaneous, sensory-evoked, photostimulation-evoked) for multiple cortical regions for each animal. We then compared sets of these seed-pixel correlation maps using spatial correlation analysis within the animals (examining how relative patterns change within a subject) which removes the necessity of registration and alignment across animals. “Sets” were defined in this context as seed-pixel correlation maps generated from the same seed-pixel location (e.g. HLS1) and by the origin of the activity from which the maps were generated (spontaneous, sensory-evoked, photostimulation-evoked) for each animal. From this we drew conclusions that some sets are relatively homogeneous (by the same seed-pixel location but obtained from different origins of activity, e.g. sHLS1, eHLS1, and pHLS1 compared with each other; Fig. 3 and Supplementary Fig. 3) and distinct from other sets (by different seed-pixel locations, but obtained from the same or different origins of activity, e.g. sHLS1, eFLS1, pFLS1; Supplementary Figs. 3 and 5). In this case the statistical significance of these comparisons depended on how consistent the individual spatial correlations were within a set (composed of up to 9 animals), and how different they were between sets. To determine statistical significance across animals, we calculated t-statistics for each comparison of one set of seed-pixel correlation maps with another set of seed-pixel correlation maps, computed using spatial correlation analysis in an identical fashion from different data (different sets across animals). For these analyses, the degrees of freedom are constrained by the number of

experimental replicates (number of mice) used for comparisons under the same experimental conditions.

To minimize the local contribution of correlation values around the seed-pixel in spatial correlation analysis, we used a 2D Gaussian fit to create a template image for each individual correlation map that models the local distribution of the correlation values centered around the seed-pixel. To exclude the contribution of the 1st order local correlations, we subtracted the template image from its corresponding original map. The resulting residual map contained only the 2nd order long-range correlation. The exclusion zone often encompass several mm in size (Supplementary Fig. 3A). We used these residual maps in our group data correlation analysis between maps obtained from evoked spontaneous, and optogenetically evoked activity (Supplementary Figs. 3B, C) as well as structure (Supplementary Fig. 6).

As an alternative method to the comparison of correlation image sets that we describe above (Supplementary Fig. 3 as an example), we have also used a region of interest based comparison of correlation index at regions identified using the combination for sensation and mouse brain atlas derived functional areas (Supplementary Fig. 4). In order to measure the amount of variance of spontaneous activity that can be accounted for by sensory motifs, we computed the mean variance (r-squared) over the whole time series of spontaneous activity (215.74 s, 0.1–6.0 Hz band-pass filtered), for each mouse.

No statistical methods were used to predetermine sample sizes, but our sample sizes are similar to those reported in previous publications[19]. Data collection and analysis were not performed blind to the conditions of the experiment. Although, experimental animals largely belonged to a single group and quantitative automated methods were employed to minimize experimenter bias. No method of randomization was used to assign animals to experimental groups. Data distribution was assumed to be normal but this was not formally tested. Error bars and ± ranges represent standard error. *, **, and *** denote $p<0.05$, $p<0.01$, and $p<0.001$, respectively. All the statistical tests were two-sided.

2D Reconstruction of axonal projection Maps

Images of 100 μm coronal sections of mice injected with fluorescent protein-expressing AAV were downloaded from the Allen Institute for Brain Science (http://connectivity.brain-map.org/) at a resolution of 2.8 μm/pixel. For each animal, a complete series of images through the entire neocortex was assembled into a 3D stack. Minor rotations and translations were applied to each image in the stack to correct slight mis-alignments, and the stack was cropped to include only the injected hemisphere, and rotated laterally 30 degrees to match the angle of the mouse head in VSD experiments. Structural data outside of cortex was masked to remove contributions from subcortical labeling, and an average intensity projection was made through the stack. To register the anatomical maps obtained from different animals, three anatomical markers of the brain were used: midline, the position of the most posterior segment of the dentate gyrus, and the position of the most anterior portion of the lateral ventricle of the injected hemisphere (right hemisphere). Because these last two positions were located within the subcortical regions of the brain, we made an orthographic projection of these positions along the vertical direction in rotated images of the cortex.

Registration of functional and anatomical maps

Functional and anatomical maps were aligned using a combination of anatomical landmarks and experimentally determined functional brain areas. Briefly, in each animal we used the position of the center of V1 sensory cortex, determined by VSD imaging, and the location of bregma, measured from the skull, to register the images with structural connectivity maps from the Allen Institute. Equivalent landmark positions from the structural data, V1 and bregma, were extrapolated from measurements of the position of the most posterior segment of the dentate gyrus and the most anterior portion of the lateral ventricle.

Supplementary Material

Refer to Web version on PubMed Central for supplementary material.

Acknowledgments

This work was supported by a Canadian Institutes of Health Research (CIHR) Operating Grant MOP-12675 (THM), a Human Frontier Science Program grant (THM), Michael Smith Foundation for Health Research postdoctoral fellowships (MHM and AWC), Heart and Stroke Foundation of Canada postdoctoral fellowships (MHM and AWC) and a CIHR Focus on Stroke postdoctoral fellowship (MHM). We thank the Allen Institute for Brain Science for providing a database of axonal projections. We thank Pumin Wang and Cindy Jiang for surgical assistance.

References

1. Zhang D, Raichle ME. Disease and the brain’s dark energy. Nat Rev Neurol. 2010; 6:15–28. [PubMed: 20057496]
2. Destexhe A, Contreras D. Neuronal computations with stochastic network states. Science. 2006; 314:85–90. [PubMed: 17023650]
3. Harris KD, Thiele A. Cortical state and attention. Nat Rev Neurosci. 2011; 12:509–523. [PubMed: 21829219]
4. Arieli A, Sterkin A, Grinvald A, Aertsen A. Dynamics of ongoing activity: explanation of the large variability in evoked cortical responses. Science. 1996; 273:1868–1871. [PubMed: 8791593]
5. Kenet T, Bibitchkov D, Tsodyks M, Grinvald A, Arieli A. Spontaneously emerging cortical representations of visual attributes. Nature. 2003; 425:954–956. [PubMed: 14586468]
6. Ferezou I, et al. Spatiotemporal dynamics of cortical sensorimotor integration in behaving mice. Neuron. 2007; 56:907–923. [PubMed: 18054865]
7. Waters J, Helmchen F. Background synaptic activity is sparse in neocortex. The Journal of neuroscience : the official journal of the Society for Neuroscience. 2006; 26:8267–8277. [PubMed: 16899721]
8. Luczak A, Bartho P, Harris KD. Spontaneous events outline the realm of possible sensory responses in neocortical populations. Neuron. 2009; 62:413–425. [PubMed: 19447096]
9. Han F, Caporale N, Dan Y. Reverberation of recent visual experience in spontaneous cortical waves. Neuron. 2008; 60:321–327. [PubMed: 18957223]
10. Vincent JL, et al. Intrinsic functional architecture in the anaesthetized monkey brain. Nature. 2007; 447:83–86. [PubMed: 17476267]
11. Leopold DA, Murayama Y, Logothetis NK. Very slow activity fluctuations in monkey visual cortex: implications for functional brain imaging. Cerebral cortex. 2003; 13:422–433. [PubMed: 12631571]
12. Lu H, et al. Rat brains also have a default mode network. Proceedings of the National Academy of Sciences of the United States of America. 2012; 109:3979–3984. [PubMed: 22355129]
13. de Pasquale F, et al. A cortical core for dynamic integration of functional networks in the resting human brain. Neuron. 2012; 74:753–764. [PubMed: 22632732]

14. Hipp JF, Hawellek DJ, Corbetta M, Siegel M, Engel AK. Large-scale cortical correlation structure of spontaneous oscillatory activity. Nature neuroscience. 2012; 15:884–890. [PubMed: 22561454]
15. Wedeen VJ, et al. Diffusion spectrum magnetic resonance imaging (DSI) tractography of crossing fibers. NeuroImage. 2008; 41:1267–1277. [PubMed: 18495497]
16. Frostig RD, Xiong Y, Chen-Bee CH, Kvasnak E, Stehberg J. Large-scale organization of rat sensorimotor cortex based on a motif of large activation spreads. The Journal of neuroscience : the official journal of the Society for Neuroscience. 2008; 28:13274–13284. [PubMed: 19052219]
17. White BR, et al. Imaging of functional connectivity in the mouse brain. PloS one. 2011; 6:e16322. [PubMed: 21283729]
18. Grinvald A, Hildesheim R. VSDI: a new era in functional imaging of cortical dynamics. Nat Rev Neurosci. 2004; 5:874–885. [PubMed: 15496865]
19. Mohajerani MH, McVea DA, Fingas M, Murphy TH. Mirrored bilateral slow-wave cortical activity within local circuits revealed by fast bihemispheric voltage-sensitive dye imaging in anesthetized and awake mice. The Journal of neuroscience : the official journal of the Society for Neuroscience. 2010; 30:3745–3751. [PubMed: 20220008]
20. OHS, et al. Allen mouse brain connectivity atlas project. Society for Neuroscience Annual Meeting Abstract. 2011:519.08/ZZ55.
21. Kleinfeld D, Delaney KR. Distributed representation of vibrissa movement in the upper layers of somatosensory cortex revealed with voltage-sensitive dyes. The Journal of comparative neurology. 1996; 375:89–108. [PubMed: 8913895]
22. Lim DH, et al. In vivo Large-Scale Cortical Mapping Using Channelrhodopsin-2 Stimulation in Transgenic Mice Reveals Asymmetric and Reciprocal Relationships between Cortical Areas. Front Neural Circuits. 2012; 6:11. [PubMed: 22435052]
23. Mao T, et al. Long-range neuronal circuits underlying the interaction between sensory and motor cortex. Neuron. 2011; 72:111–123. [PubMed: 21982373]
24. Grandy TH, Greenfield SA, Devonshire IM. An evaluation of in vivo voltage-sensitive dyes: pharmacological side effects and signal-to-noise ratios after effective removal of brain-pulsation artifacts. Journal of neurophysiology. 2012; 108:2931–2945. [PubMed: 22972958]
25. Akemann W, et al. Imaging neural circuit dynamics with a voltage-sensitive fluorescent protein. Journal of neurophysiology. 2012; 108:2323–2337. [PubMed: 22815406]
26. Liu, C. Beyond pixels : exploring new representations and applications for motion analysis. Massachusetts Institute of Technology; 2009. p. 164
27. Takagaki K, Zhang C, Wu JY, Ohl FW. Flow detection of propagating waves with temporospatial correlation of activity. Journal of neuroscience methods. 2011; 200:207–218. [PubMed: 21664934]
28. Bullmore E, Sporns O. Complex brain networks: graph theoretical analysis of structural and functional systems. Nat Rev Neurosci. 2009; 10:186–198. [PubMed: 19190637]
29. Poulet JF, Petersen CC. Internal brain state regulates membrane potential synchrony in barrel cortex of behaving mice. Nature. 2008; 454:881–885. [PubMed: 18633351]
30. Haider B, Hausser M, Carandini M. Inhibition dominates sensory responses in the awake cortex. Nature. 2013; 493:97–100. [PubMed: 23172139]
31. Polack PO, Contreras D. Long-range parallel processing and local recurrent activity in the visual cortex of the mouse. The Journal of neuroscience : the official journal of the Society for Neuroscience. 2012; 32:11120–11131. [PubMed: 22875943]
32. Huang X, et al. Spiral wave dynamics in neocortex. Neuron. 2010; 68:978–990. [PubMed: 21145009]
33. Sato TK, Nauhaus I, Carandini M. Traveling waves in visual cortex. Neuron. 2012; 75:218–229. [PubMed: 22841308]
34. Niell CM, Stryker MP. Modulation of visual responses by behavioral state in mouse visual cortex. Neuron. 2010; 65:472–479. [PubMed: 20188652]
35. Wilson MA, McNaughton BL. Reactivation of hippocampal ensemble memories during sleep. Science. 1994; 265:676–679. [PubMed: 8036517]
36. Euston DR, Tatsuno M, McNaughton BL. Fast-forward playback of recent memory sequences in prefrontal cortex during sleep. Science. 2007; 318:1147–1150. [PubMed: 18006749]

37. Douglas RJ, Martin KA. Mapping the matrix: the ways of neocortex. Neuron. 2007; 56:226–238. [PubMed: 17964242]
38. Reid RC. From functional architecture to functional connectomics. Neuron. 2012; 75:209–217. [PubMed: 22841307]
39. Shmuel A, Leopold DA. Neuronal correlates of spontaneous fluctuations in fMRI signals in monkey visual cortex: Implications for functional connectivity at rest. Human brain mapping. 2008; 29:751–761. [PubMed: 18465799]
40. Grienberger C, et al. Sound-evoked network calcium transients in mouse auditory cortex in vivo. The Journal of physiology. 2012; 590:899–918. [PubMed: 22106174]
41. Buzsaki G, et al. Nucleus basalis and thalamic control of neocortical activity in the freely moving rat. J Neurosci. 1988; 8:4007–4026. [PubMed: 3183710]
42. Beier KT, et al. Anterograde or retrograde transsynaptic labeling of CNS neurons with vesicular stomatitis virus vectors. Proceedings of the National Academy of Sciences of the United States of America. 2011; 108:15414–15419. [PubMed: 21825165]
43. Osakada F, et al. New rabies virus variants for monitoring and manipulating activity and gene expression in defined neural circuits. Neuron. 2011; 71:617–631. [PubMed: 21867879]
44. Cardin JA, et al. Driving fast-spiking cells induces gamma rhythm and controls sensory responses. Nature. 2009; 459:663–667. [PubMed: 19396156]
45. Tamamaki N, Tomioka R. Long-Range GABAergic Connections Distributed throughout the Neocortex and their Possible Function. Frontiers in neuroscience. 2010; 4:202. [PubMed: 21151790]
46. Alivisatos AP, et al. The brain activity map project and the challenge of functional connectomics. Neuron. 2012; 74:970–974. [PubMed: 22726828]
47. Bohland JW, et al. A proposal for a coordinated effort for the determination of brainwide neuroanatomical connectivity in model organisms at a mesoscopic scale. PLoS computational biology. 2009; 5:e1000334. [PubMed: 19325892]
48. Li A, et al. Micro-optical sectioning tomography to obtain a high-resolution atlas of the mouse brain. Science. 2010; 330:1404–1408. [PubMed: 21051596]
49. Kleinfeld D, et al. Large-scale automated histology in the pursuit of connectomes. The Journal of neuroscience : the official journal of the Society for Neuroscience. 2011; 31:16125–16138. [PubMed: 22072665]
50. Azin M, Guggenmos DJ, Barbay S, Nudo RJ, Mohseni P. A miniaturized system for spike-triggered intracortical microstimulation in an ambulatory rat. IEEE Trans Biomed Eng. 2011; 58:2589–2597. [PubMed: 21690007]
51. Shoham D, et al. Imaging cortical dynamics at high spatial and temporal resolution with novel blue voltage-sensitive dyes. Neuron. 1999; 24:791–802. [PubMed: 10624943]
52. Paxinos, G., Franklin, KBJ. The mouse brain in stereotaxic coordinates. Elsevier Academic Press; Amsterdam ; Boston: 2004.

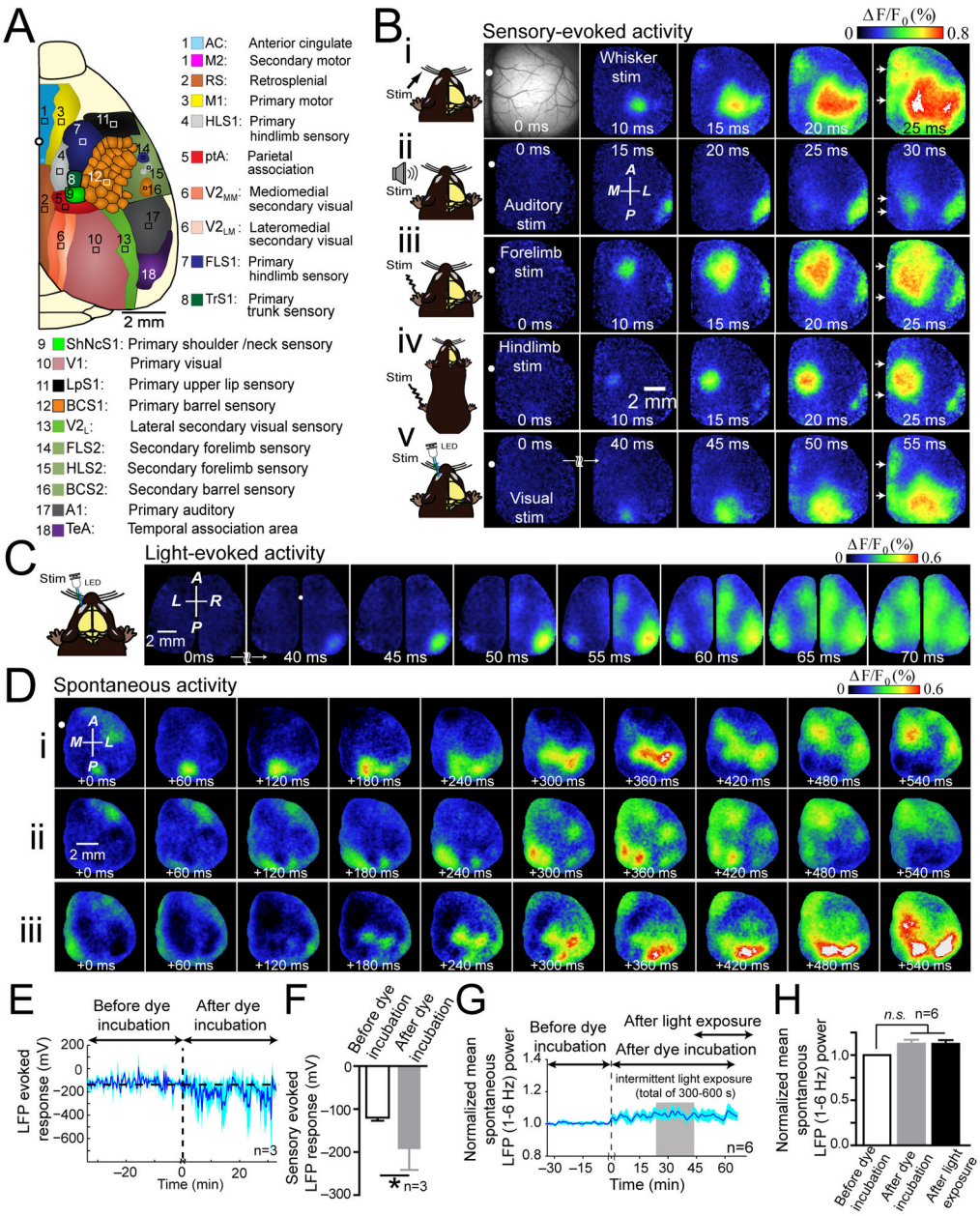

Figure 1. Unique and consensus activation patterns during multiple forms of sensory stimulation

(A) Schematic of unilateral craniotomy showing imaged cortical regions. **(B)** Photomicrograph of wide unilateral craniotomy, with bregma marked as white circle (top, left). Patterns of cortical activation following (i) stimulation of contralateral C2 whisker, (ii) auditory stimulation, (iii) contralateral forelimb stimulation, (iv) contralateral hindlimb stimulation, and (v) visual stimulation of contralateral eye in isoflurane (0.5%) anesthetized mouse. Note midline activation after all sensory stimulation forms (white arrows), 10–25 ms following primary sensory cortex activation. Responses are mean of 20 trials. Second panel of VSD responses in second row shows anterior (A), posterior (P), medial (M) and lateral (L) directions. (C) Representative montage of VSD response following visual stimulation of

left eye in bilateral craniotomy. Responses are mean of 10 trials. **(D)** (i–iii) Three sequences of spontaneous cortical activity in an anesthetized mouse. See Supplementary Figs. 1, and 4 for group data analysis. (**E)** Time course of the amplitude of repeated (0.05 Hz), forelimb sensory stimulation-evoked responses measured from an LFP electrode placed within FLS1 before and after RH1692 dye loading. (**F)** Summary of mean peak amplitude in **E. (G)** Time course of normalized mean spontaneous LFP power. Recording resumed 30 min following RH1692 washout to encompass periods prior to, during, and after intermittent VSD excitation (denoted as light exposure; total illumination time 300–600 s). (**H)** Summary of LFP power in **G**. Error bars represent s.e.m.

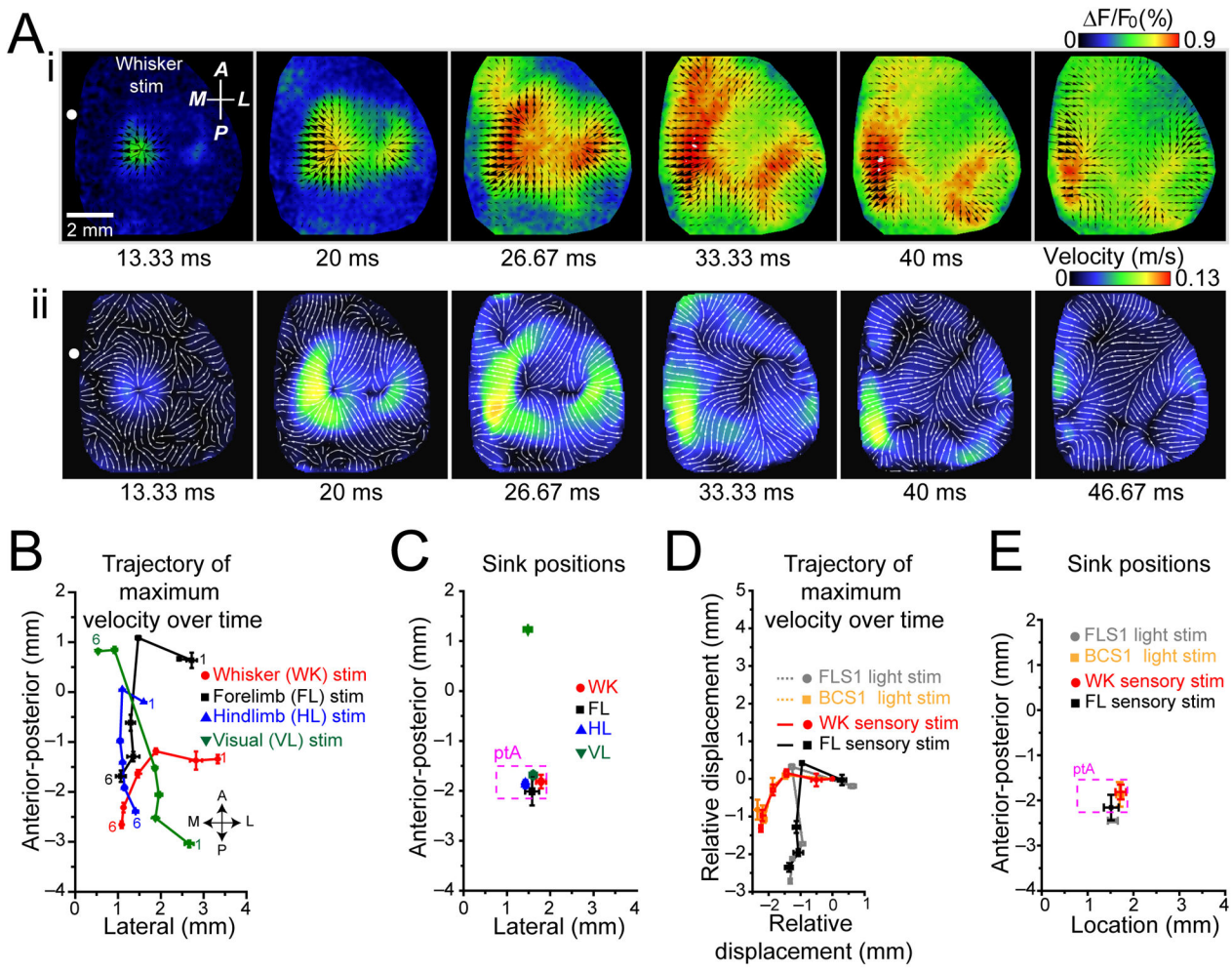

Figure 2. Sensory and photostimulation-induced activation exhibit modality specific source locations and termination at a common sink location

(A)(i) Whisker stimulation-evoked VSD activation (average of 20 trials). Black arrows indicate the direction of velocity of VSD signal spread. Relative magnitude of velocity is indicated by arrows size. (ii) For response in (i), measurements of absolute velocity are represented in pseudocolor. Streamlines indicate local direction of velocity flow. **(B)** Position of maximum velocity (center of mass) of VSD signal spread from sensory stimulation following initial activation on cortex relative to bregma at six 6.67 ms intervals indicated as 1 to 6. Bregma is at coordinate (0,0). **(C)** Position of sink locations for each sensory modality plotted on cortex relative to bregma. All forms of sensory stimulation shared a common sink location within parietal association area (ptA), dotted box ($p>0.05$, n=8 mice). Visual stimulation resulted in an additional, sink location within anterior medial cortex (***$p<0.001$, n=8 mice). **(D)** Positions of maximum velocity of VSD signal spread following sensory (forelimb and whisker) and photostimulation (FLS1 and BCS1). Maximum velocity positions for each trajectory were normalized to their initial positions. Trajectories from sensory stimulation and photostimulation were similar ($p>0.05$, for sensory versus photostimulation of the same of modalities, n=7 mice). **(E)** Positions of sink locations for sensory and photostimulation-induced activation plotted on cortex relative to

bregma. Sink locations between sensory-evoked and photostimulation induced activation were similar ($p>0.05$ for all comparisons, $n=7$ mice). Error bars represent s.e.m.

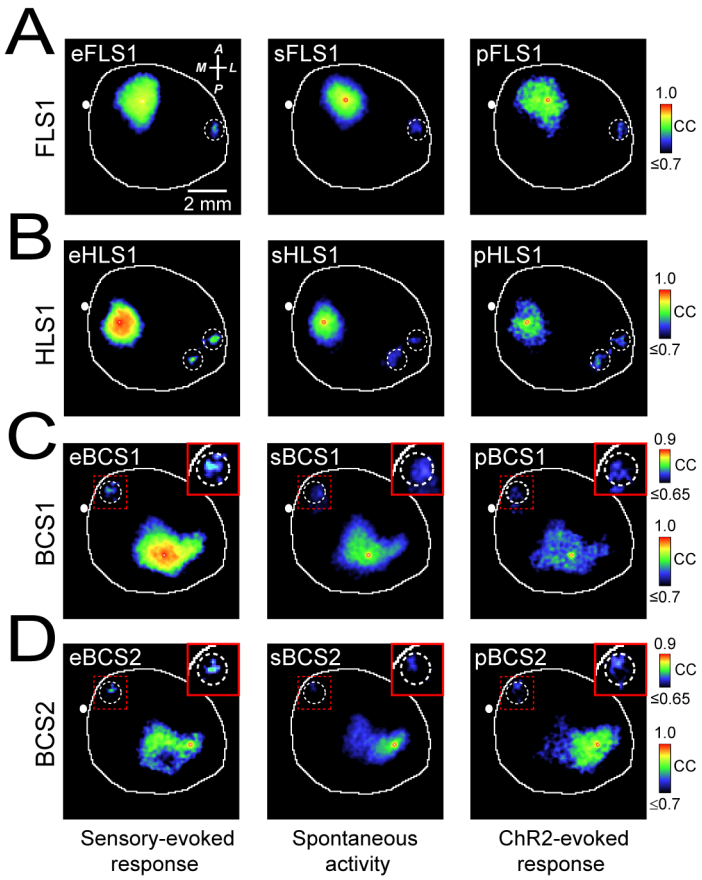

Figure 3. Spontaneous, sensory-, and photostimulation-evoked cortical VSD maps share similar regional patterns

(A) Representative correlation maps from a seed-pixel located within the primary representation of forelimb somatosensory cortex (FLS1) generated from VSD signals after sensory stimulation of contralateral forelimb (eFLS1, left), during 300 s of cortical spontaneous activity (sFLS1, center), or after direct photostimulation of FLS1 (pFLS1, right). **(B–D).** Similar to **A** but locating the seed-pixel within **(B)** primary representation of hindlimb cortex (HLS1), **(C)** primary representation of C2 barrel cortex (BCS1), or **(D)** secondary representation of C2 barrel cortex (BCS2). Inset images represent magnification of area denoted by dotted red box and were all re-scaled to the upper calibration bar. Position of bregma marked as white circle. Compass arrows indicate anterior (A), posterior (P), medial (M) and lateral (L) directions. Note that the correlation coefficients (CC) are color-coded. See Supplementary Figs. 3, 5 for group data analysis.

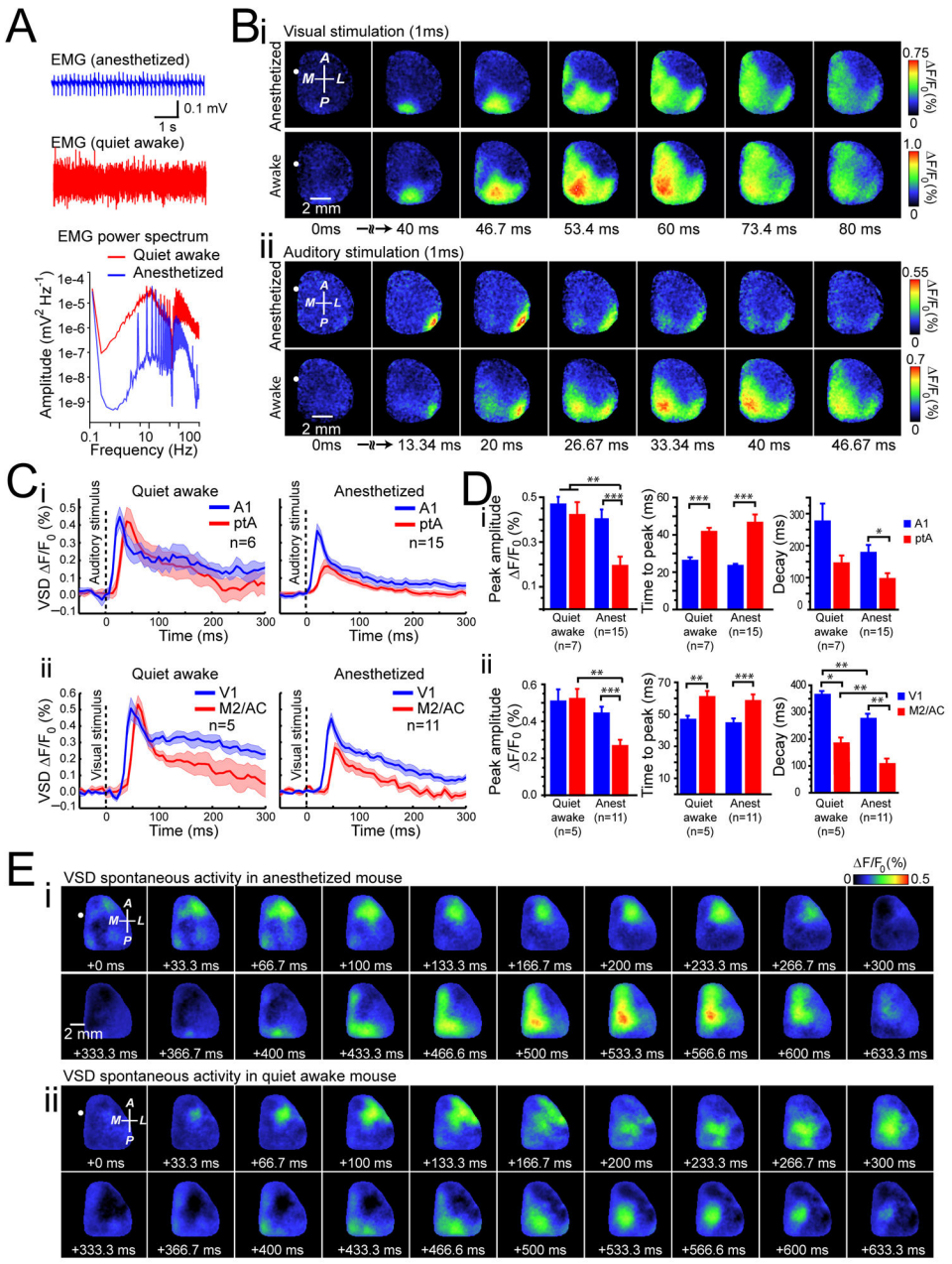

Figure 4. Patterns of sensory-evoked and spontaneous activity in quiet awake mice are similar to those observed under anesthesia

(A) Individual example of neck muscle electromyography (EMG) (>1 Hz) from a head-restrained mouse under isoflurane (0.5%) anesthesia (top trace), or 1 h after awakening (bottom trace). The power spectrum of the EMG signals show different spectra between states of anesthesia (blue) and wakefulness (red). **(B)** Representative cortical VSD signals in response to contralateral (i) visual or (ii) auditory stimulation during anesthesia (top panel) or in quiet awake states (bottom panel). Images represent the average of 10 trials of stimulation. Note that responses are scaled differently. **(C)** Quantification of VSD signals to (i) auditory stimulation or (ii) visual stimulation in anesthetized (right panels) or quiet awake

states (left panels). Plots are average of VSD signals measured from 5 × 5 pixel boxes (~ 0.11 mm^2) placed within (i) A1 (blue traces) and ptA (red traces) for auditory stimulation, or (ii) V1 (blue traces) and M2/AC (red traces) for visual stimulation. **(D)** Statistical quantification of peak amplitude (left panels), time to peak (center panels), and decay (right panels) of the (i) auditory-evoked or (ii) visual-evoked VSD responses during anesthesia or quiet awake states. **(E)** Representative montages showing two distinct time epochs (each 633.3 ms) of VSD imaging of spontaneous cortical activity during (i) anesthesia, (ii) or in a quiet awake states. Position of bregma marked as white circle. Compass arrows indicate anterior (A), posterior (P), medial (M) and lateral (L) directions. Error bars represent s.e.m.

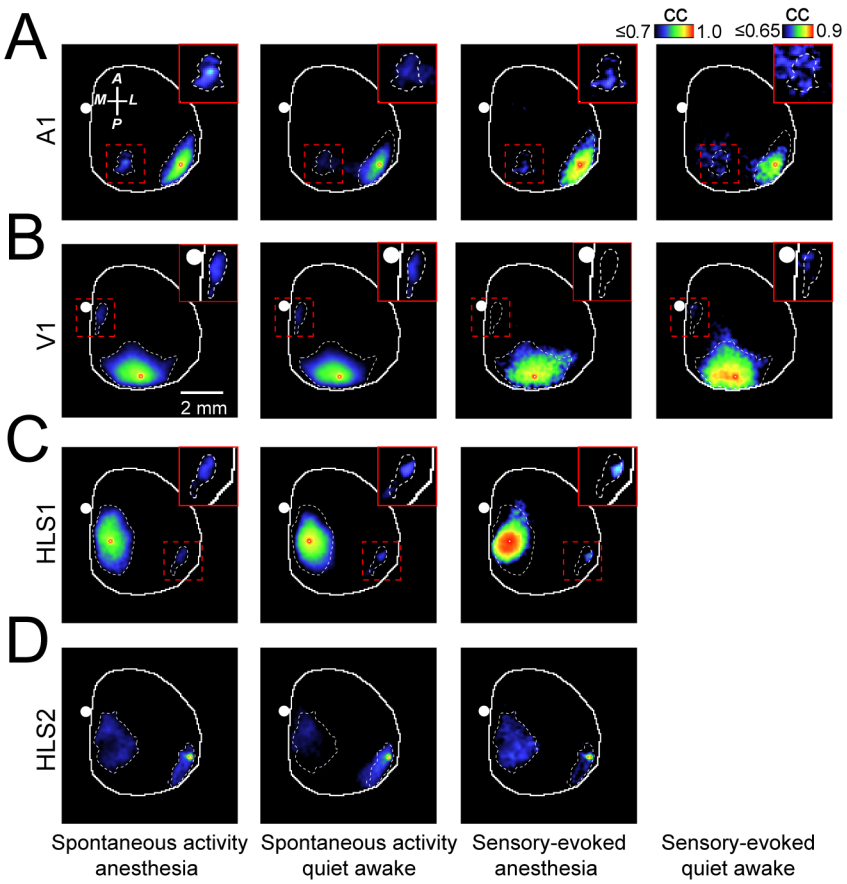

Figure 5. Correlation maps generated from sensory-evoked or spontaneous activity during quiet wakefulness are similar to maps obtained during anesthesia

(A) Representative correlation maps generated from a seed-pixel from primary auditory cortex (A1) calculated from 300s of cortical spontaneous activity in isoflurane induced anesthesia (1st column from left), quiet wakefulness (2nd column from left) or after auditory stimulation in anesthetized or quiet awake states (3rd and 4th column from left respectively). Inset images represent magnification of area denoted by dashed red box and were all re-scaled to the right calibration bar. **(B–D)** Similar to **A**, the correlation maps were calculated within primary visual cortex (V1) **(B)**, primary representation of hindlimb somatosensory cortex (HLS1) or secondary representation of hindlimb somatosensory cortex (HLS2) **(C, D)**. CC denotes correlation coefficient. Position of bregma marked as white circle. Compass arrows indicate anterior (A), posterior (P), medial (M) and lateral (L) directions. See Supplementary Fig. 7 for group data analysis.

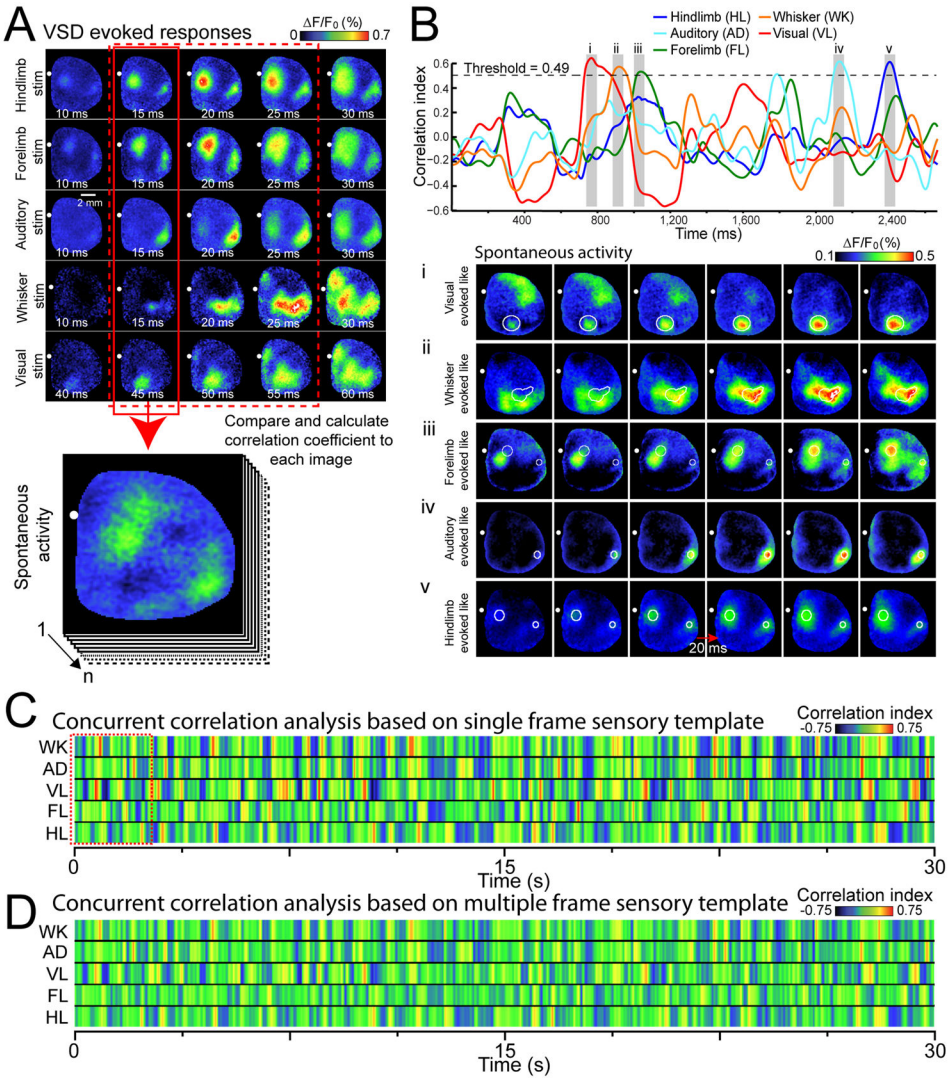

Figure 6. Spontaneous cortical activity can be decomposed into unique repeating sensory motifs

(A) Representative montages show examples of VSD response to five different forms of sensory stimulation. Each image of spontaneous activity was compared with the sensory evoked templates (pattern at initial cortical response, highlighted by solid red box). VSD responses represent the average of 20–45 trials of stimulation. **(B)** Top, plot of concurrent correlation of instantaneous patterns of spontaneous activity (2.6 s of spontaneous VSD data as denoted by red dashed square in **C** with multiple templates of sensory evoked responses. Spontaneous activity was considered to be a “match” to the evoked template if the correlation value was greater than a given threshold (see Supplementary Fig. 8A). Bottom, representative montages (20 ms intervals) showing cortical spontaneous activity that resembles sensory stimulation derived templates, corresponding to shaded gray regions highlighted in the top panel. **(C)** Pseudocolor image representing a 30 s time course of concurrent correlation of different templates of sensory evoked responses (rows representing whisker (WK), auditory (AD), visual (VL), forelimb (FL), and hindlimb (HL)) with a 30 s epoch of spontaneous activity. The color of each column of pixels represents the correlation

value at different times. **(D)** Concurrent correlation as in **C**, but using templates of sensory-evoked responses containing the first three frames of sensory-evoked activity following the initial response (highlighted by dashed red box in A).

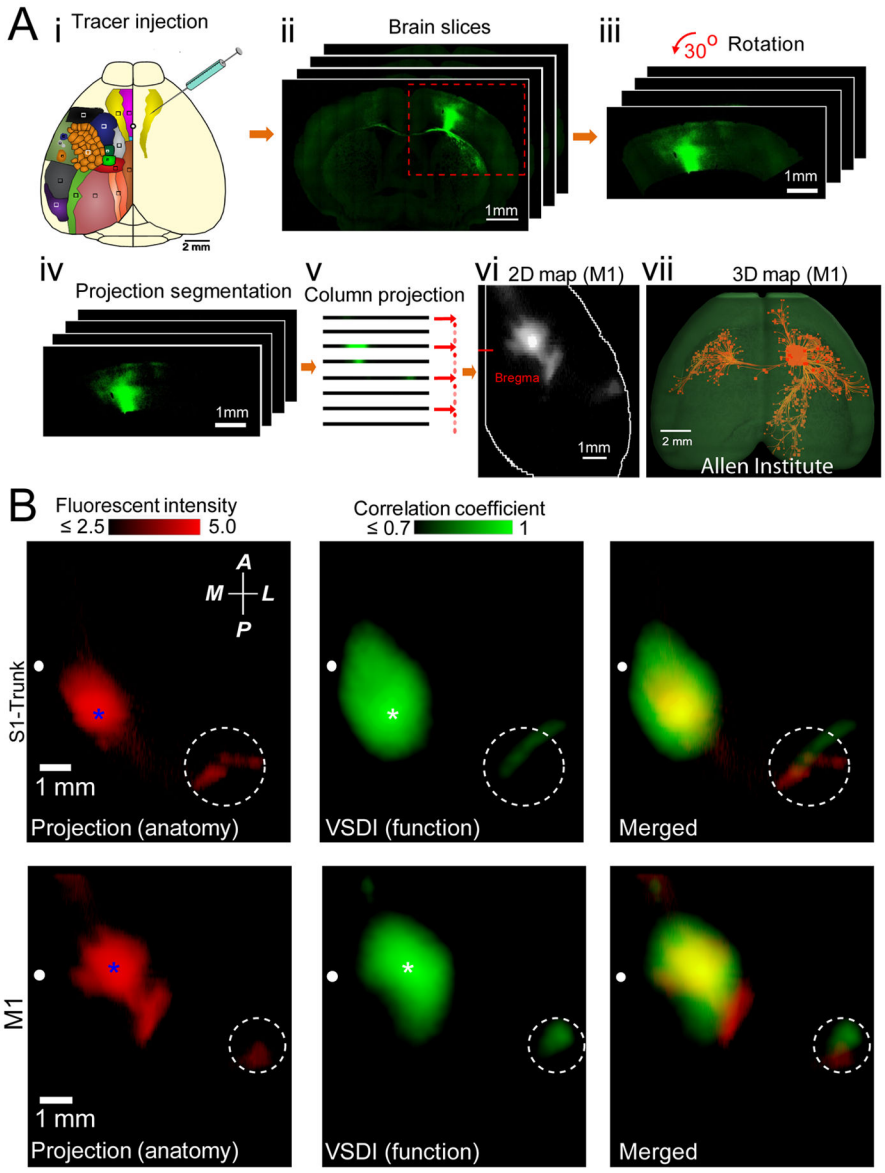

Figure 7. Comparison of cortical axonal projection patterns to correlation maps of spontaneous cortical activity

(A)(i). Schematic showing injection of AAV tracer to map axonal projections of different cortical regions within the adult mouse brain (data obtained from the Allen Institute for Brain Science). Color-coded cortical locations are as described in Fig. 1. To quantitatively compare the axonal projection maps with functional correlation maps, 2D representations of Allen Mouse Brain Connectivity datasets were created (ii–vi**,** See Methods). (vii) 3D reconstruction, using Brain Explorer software from Allen Institute for Brain Science, of primary motor cortex axonal projections. **(B)** Left, example of primary somatosensory trunk (S1-Trunk) and primary motor (M1) cortex axonal projection maps are shown. Pixel intensities scaled logarithmically. Seed-pixel correlation maps obtained from VSD imaging of spontaneous activity within S1-Trunk or M1 cortex are shown in center. Spatial co-localization of axonal projection (left) and correlation (center) maps are shown in right.

White dashed circles indicate position of secondary somatosensory cortex. Blue and white stars indicate positions of tracer injection and the seed-pixel, respectively. Position of bregma marked as white circle. Compass arrows indicate anterior (A), posterior (P), medial (M) and lateral (L) directions. See Fig. 8 for group data analysis.

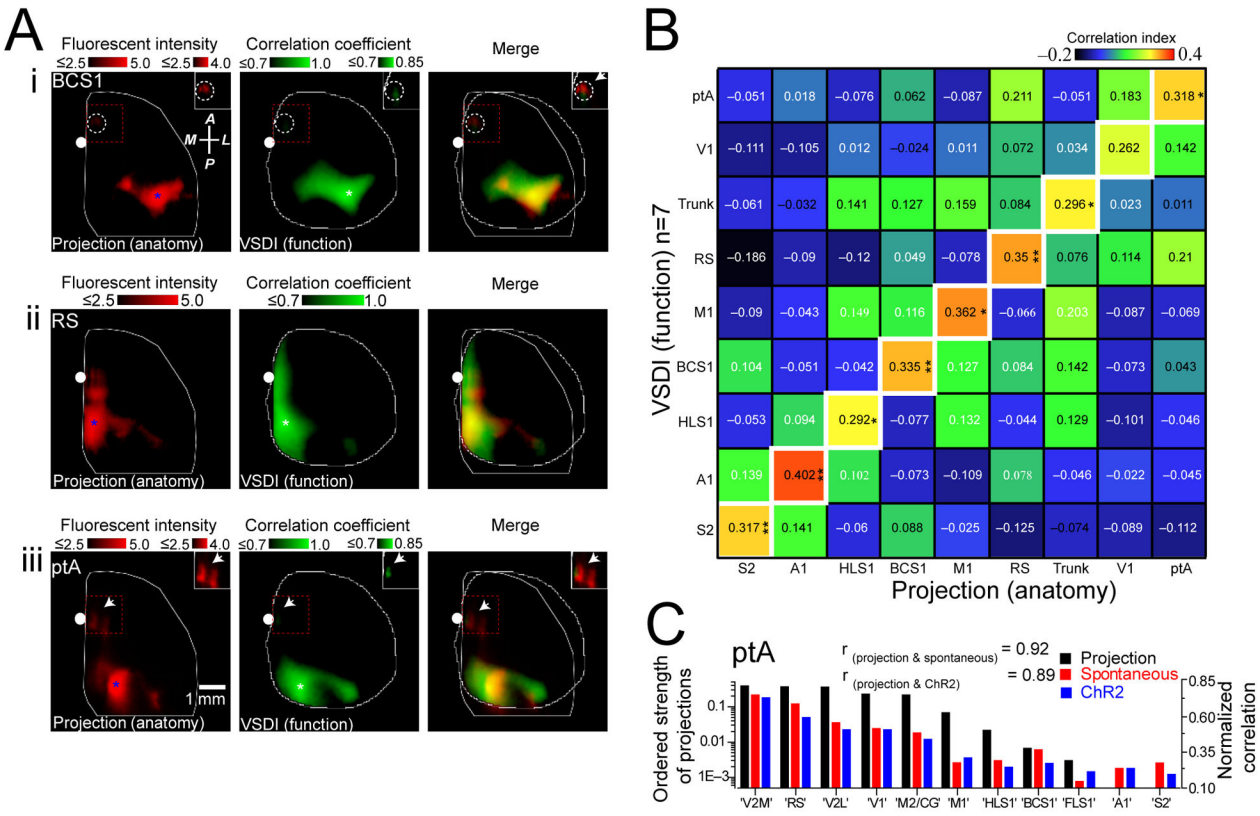

Figure 8. Axonal projection maps are most similar to their corresponding functional maps

(A)(i) Axonal projection maps (left) of primary barrel somatosensory cortex (BCS1). Blue asterisk denotes AAV injection site. Pixel intensities scaled logarithmically. Note relatively weak pixel intensity in the area outside the injection site (dashed circle). Seed-pixel correlation map (center; presumed similar location to AAV injection site) of BCS1 obtained from spontaneous activity. White asterisk denotes location of seed-pixel. Right, overlay of anatomical and correlation maps. Inset images represent the areas denoted by dashed red boxes and were all re-scaled to the upper right calibration bars. Similar to (i), axonal projection and correlation maps shown for (ii) retrosplenial cortex (RS) and (iii) parietal association cortex (ptA). **(B)** Matrix showing similarity between VSD correlation (n=7 mice) and axonal projection maps for nine cortical regions. **(C)** Ordered strength of ptA axonal projections (black) to eleven regions of interest (ROIs) compared to normalized correlation maps obtained from spontaneous activity (red; n=10 mice) or ChR2-evoked VSD responses (blue; n=6 mice). ROIs are ordered based on strength of ptA axonal projection density to other ROIs. The rank order of axonal projection strength was similar to the rank order of functional connectivity strength measured from both spontaneous activity and ChR2-evoked responses ($r_{projection(ptA)\&spontaneous(ptA)} = 0.92$, $r_{projection\ (ptA)\&ChR2(ptA)} = 0.89$, $p<0.001$ both comparisons). Tests of significance were made against a null hypothesis of axonal projection strength and HL functional connectivity strength ($r_{projection(ptA)\&spontaneous(HLS1)}=-0.37$, $r_{projection(ptA)\&ChR2(HLS1)} = -0.38$, $p>0.20$ both comparisons).